Volume 1 | Number 1 | Jan 2013 | Pages 1–100

ChemComm

Chemical Communications
www.rsc.org/chemcomm

ROYAL SOCIETY OF CHEMISTRY

www.rsc.org/chemcomm

Journal Name

COMMUNICATION

Loading of Mesosporous Titania films by CH₃NH₃PbI₃ Perovskite, Single step vs Sequential deposition

Natalia Yantara[+ ab], Sabba Dharani[+ ab], Fang Yanan[b], Jeannette M. Kadro[ac], Thomas Moehl,[*d] Pablo P. Boix,*[a] Subodh Mhaisalkar,[ab] Michael Grätzel,[d] and Carole Grätzel[*d]

Infiltration of mesoporous TiO₂ scaffolds by CH₃NH₃PbI₃ is more complete when using sequential compared to single step deposition processing and avoids formation of disordered capping layers affording greatly improved performance of perovskite based photovoltaics.

Worldwide the photovoltaic community's attention is presently focused on the promising properties of the perovskite class of compounds as both light absorbers and as charge (both electron and hole) transport materials.[1-5] The highest certified solar to electrical power conversion efficiency (PCE) value under AM 1.5G sunlight conditions has recently reached 20.1%.[6-9] These inorganic or mixed organic-inorganic compounds can likewise be exploited in other electronic devices such as LEDS, photodetectors, transistors as well as for laser applications.[10-13] Their ease of formation with readily available and inexpensive compounds as well as diverse fabrication techniques leads to multitudes of different and easily obtainable structures.

Recently several preparation methods have been exploited to fabricate perovskite photovoltaic devices with high and easily reproducible performance.[6-8] The variation of the electron and hole selective layers[14, 15] has been an effective approach. Additionally various mesoscopic oxides, either isolating, such as Al₂O₃, or electron transporting, e.g. TiO₂ and ZnO have been employed as scaffolds/electron transporters for these photovoltaic devices[1, 4, 16]. In this manuscript we concentrate on the domain of solid-state sensitized inorganic-organic hybrid photovoltaic devices' fabrication, more specifically utilizing the methylammonium lead iodide perovskite (CH₃NH₃PbI₃) solid-state version of the well-known TiO₂ mesoscopic film based DSC. We compare the two most extensively utilized methods of perovskite deposition: single step from a DMF[1] solution and sequential deposition.[3,17] Processing techniques of the perovskites are critical to obtain highly efficient photovoltaic devices, with the sequential deposition method generating more efficient devices as previously reported[17].

Homogeneous and conformal layer formation as well as an optimal thickness of the perovskite films fabricated and their concomitant capping layers are primordial to achieve high performance. Distortions and defects of the crystal lattices and grain boundaries can be deleterious to the efficient functioning of this type of solar cell device.[6, 18]

Here we analyze the effect of the deposition method on the morphology and PV performance of CH₃NH₃PbI₃ based solar cells. Differences in the perovskite's formation and functionality resulting from the application of two types of deposition techniques on devices comprised of TiO₂ mesoscopic films are examined with MAPbI₃ perovskite as light harvester and spiro-OMeTAD as hole transport material. Systematic studies involving a single-step deposition technique at various precursor concentrations in DMF (dimethylformamide), i.e., 20, 30 and 40 wt%, and the sequential step deposition method outlined in the work by Burschka, et al,[3] have been undertaken. A comparative study of SEMs, TEMs, JV curves, IPCE and impedance spectra (IS) measured under illumination for these solid-state sensitized mesoscopic inorganic-organic hybrid solar cells is presented.

For the single-step perovskite formation various concentrations (i.e., 20 wt%, 30 wt% and 40 wt%) were prepared by mixing CH₃NH₃I and PbI₂ (99%, Aldrich) in 1:1 molar ratio in dimethylformamide (DMF) at various dilutions and left overnight under stirring at 70ºC. They were then spin-coated onto the TiO₂ mp-films at 2000rpm for 60s and annealed for 30 min at 100Cº. For the sequentially deposited MAPbI₃ perovskite the procedure followed is similar to that outlined in the publication of Burschka, et al. PbI₂ (1M) was dissolved in DMF (461 mg of PbI2 in 1 mL of DMF) overnight and left under stirring at 70 °C. The solution was spin-coated onto the mesoporous TiO₂ scaffold using a rotation speed of 6000 rpm and subsequently dried at 70 °C for a period of 30 minutes in nitrogen atmosphere. The films were then dipped in a solution of CH₃NH₃I solubilized in 2-propanol (10mg/ml) for approximately 20 min, followed by rinsing with 2-propanol,

and then dried at 70° C for 30 min in a dry air condition with humidity level < 15%.

All of the devices fabricated utilized the same procedure for the TiO_2 mesoporous film and blocking layer formation, as well as hole transporting material (HTM) which, are outlined in the experimental section of this manuscript in the supporting information (SI).
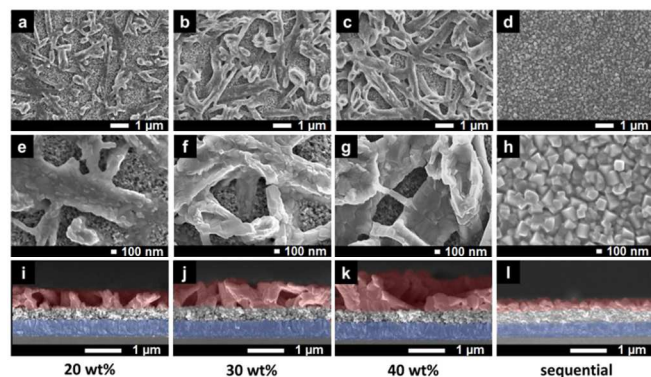

Figure 1 Scanning electron microscope images (top and cross-sectional views): Top views (**a,b,c** (1 µm scale) **e,f,g** (100 nm scale) and cross-sectional views (**i,j,k**) (1 µm bottom scale) of the MAPbI3 perovskite formed from 20 wt% (**a,e,i**), 30 wt% (**b,f,j**) and 40wt% (**c,g,k**) precursor solutions in DMF and sequentially deposited perovskites, top views (**d, h** at 1 µm, 100 nm scale) and cross-sectional view (**l** at 1 µm bottom scale) deposited on top of mp-TiO_2 films where the perovskite overlayer is shaded in red and the FTO is shaded in blue.

Investigations by SEM and TEM have been undertaken to better understand the morphology and conformity changes when using different concentrations of precursors in the perovskite single-step deposition method and compared to the sequential deposition technique. In Figure 1a-c, e-g, i-k, the topographical and cross-sectional SEM views exhibit the difference in perovskite structures on the TiO_2 film substrate when a single-step deposition technique is utilized at different perovskite precursor concentrations in DMF. Figure 1d, h, i show the top and cross-sectional SEM views of films produced by the sequential technique. The comparison of the SEM images using these two different deposition techniques clearly depicts substantial differences in morphology and conformal coverage of the TiO_2. As is observed in Fig 1a-c the perovskite's particulate network is more branchlike in appearance, and the surface coverage on the TiO_2 film is less complete (at all of the various concentrations of precursor solutions utilized) than found in the case of the perovskite formed using the sequential deposition technique. Clearly observable is the fact that the interconnectivity improves at higher concentrations of the precursor solutions for the branched like structures of the capping over-layers as well as does the coverage of the mesoporous TiO_2. The "branches" also protrude more from the surface as the precursor concentration increases. Although the coverage increases with higher wt% in the precursor solution, the access to the TiO_2 film surface by the HTM is likely less limited through these films, than it is in the sequentially deposited MAPbI$_3$ perovskite films. The enhancement of pore filling of the TiO_2 film by perovskite with an increase in precursor concentration in the one step method is not evident from these measurements. A better pore filling in the mesoporous metal oxide

film is observed when the perovskite is deposited by the two-step method. In the sequentially deposited perovskite film, the crystal formation appears to be more particulate (cubic shape) and compact in nature, suggesting that the access to the TiO_2 film surface by the hole conductor is limited both by the conformal and homogeneous deposition of a significant perovskite over (capping)-layer. It should be noted that the perovskite capping layer is not only more compact using the sequential deposition method, but also that the thickness is much more homogeneous than in the single step deposited films. This phenomenon is clearly observed in the SEM images corresponding to the cross section of the films (Figure 1i-l). The films by the one step method are deposited in irregular forms and varying thicknesses for each precursor concentration utilized. The average film thickness increases as a function of the concentration of the precursor in the single step deposition from ~0.5 µm (Figure 1e) in the 20% sample to more than 1 µm in the 40% one (Figure 1k). In contrast, the sequentially deposited film has an evenly deposited capping layer of ~0.3-4 µm (see Figure 1l)

This disparity of perovskite film structures is preserved in the morphology of the full devices, Figure 2a, b showing the cross-sectional SEM images for full solar cell devices with MAPbI$_3$ obtained for a) the 40% single-step and b) the sequentially deposited techniques. While the sequentially deposited device has an almost layered-type structure onto which the HTM coats as a flat surface covering the absorber (Figure 2b) the single step solar cells exhibit a very irregular surface translating the rough morphology of the perovskite into the structure of the HTM and the final solar cell device (Figure 2a). Also clearly visible in Fig. 2a is the fact that vast areas of the mp-TiO_2 are in close contact with the HTM while in Fig. 2b following sequential deposition a definitive separation of the HTM from the mp-TiO_2 by the perovskite can be observed. However, it is worthwhile to note that complete coverage of the perovskite is achieved in all the cases by the HTM.
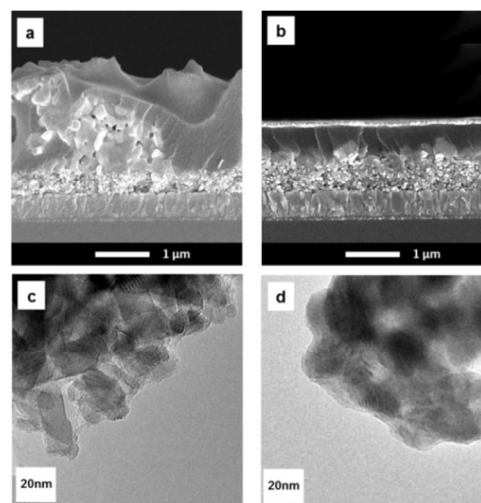
Figure 2 SEM images (cross-sectional views) of MAPbI$_3$ perovskite deposited by **(a)** single-step deposition, and **(b)** by sequential deposition in complete devices and TEM images of **(c)** single-step (40%) and **(d)** sequential deposition films.

The TEM analysis (Figures 2c,d), shows that the sequential deposition affords a conformal coverage of the TiO_2 particles by the $MAPbI_3$ combined with enhanced pore infiltration (a TEM image of bare TiO_2 film is shown in Figure S3 for reference). By contrast, one step deposition results in less complete coverage and part of the surface of the anatase nanocrystals remain exposed. Apparently, the sequential and single step methods result in very different perovskite overlayers and pore filling. Thus, apart from the pore filling, a factor that should enhance a charge percolation pathway, the dense coating of the TiO_2 nanocrystals and the regularity of the perovskite capping layers appear primordial to obtain enhancements in PECs.

The performance of the devices under AM1.5G illumination is illustrated in Figure 3 and Table 1. Although a clear trend for the short circuit currents (Jsc) is obtained for the different precursor concentration solutions used in the single step deposition ($J_{sc,40\%}$ > $J_{sc,30\%}$ > $J_{sc,20\%}$), in good agreement with the EQEs in Figure 4b, similar open circuit potential (Voc) is obtained for these samples. This increase in the EQE is expected due to the higher loading of the perovskite onto the mesoporous TiO_2 as visible in Figure 1a-c. The situation is different for the sequentially deposited solar cell, which achieves a slightly higher Jsc than its 40% single deposited counterpart, but with a better fill factor and higher Voc. The EQE spectra for the one step deposition reflect the trend observed for the Jsc, however the integrated photocurrent (Jsc-int) show lower values than the photocurrent from the JV curve (see Table 1). Clearly, the Jsc vs. Jsc-int mismatch is lower, and the EQE values are superior, for the cells prepared by the sequential method due to enhanced light harvesting and charge carrier collection, which is also suggested by the more pronounced hysteresis for the devices made by one step method. (see supporting information Figure S1). The disparity between the integrated and the current-voltage Jsc, especially for the single step samples, is attributed to a combination of the irregular perovskite overlayer and the lower perovskite conductivity observed in the dark[19], which hinders the charge collection during the EQE measurement (in contrast to the jV curve, measured under 1 sun illumination).
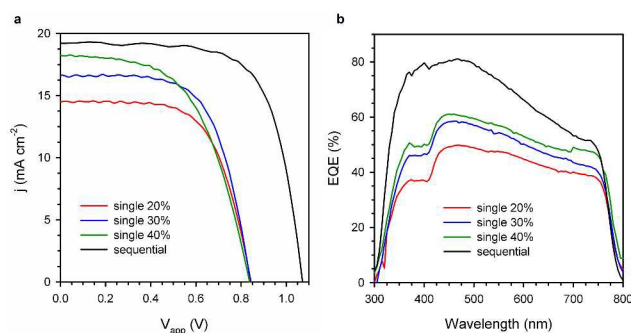
Figure 3 Representative examples of JV curves **(a)** and IPCEs **(b)** for solar cells fabricated by different precursor solution concentrations and sequential deposition.

In order to further elucidate the different device performance we carried out impedance spectroscopy (IS) under one sun illumination. The complete model for an equivalent circuit for such perovskite solar cell devices is still under discussion, especially since there is

such a variety of device designs presently encountered. The devices from the single step method investigated here are similar to the ones investigated by Dualeh et al. that show the charge accumulation occurs within the TiO_2.[20] On the other hand the devices by the two step (or evaporation) method seem to show charge accumulation taking place inside of the perovskite.[21, 22]

Table 1 Performance parameters of representative solar cells fabricated by sequential and single step deposition methods. Jsc corresponds to the short circuit current integrated form the EQE

Deposition	Jsc (mA/cm2)	Jsc int* (mA/cm2)	Voc (V)	FF	η (%)
Sequential	19.2	16.7	1.07	0.69	14.3
20 wt%	14.5	11.1	0.84	0.64	7.8
30 wt%	16.6	12.6	0.84	0.64	8.9
40 wt%	18.6	13.5	0.83	0.55	8.5

In Fig. 4 we present the resistance and the associated capacitance extracted from the low frequency response. The resistance (R_{rec}) clearly mirrors the shape of the JV curve showing slower recombination behaviour of the devices made by the sequential deposition technique, especially at higher forward bias, explaining the higher Voc obtained with this technique. This observation is in good agreement with the dark current behaviour (see supporting information Figure S2), where the onset of current flow for the sequentially deposited sample is noticeably shifted towards higher bias potential. Interestingly the R_{rec} for the single step method reduces at higher concentrations in the precursor solution. This reduction is supported by the SEM pictures of the one step deposition, where one can observe that the crystallites on top of the TiO_2 layer protrude more from the surface as the precursor concentration augments and, therefore, lead to; i) an increase in contact area between the perovskite and the HTM; ii) increased probability of a contact between the perovskite and the gold and iii) to a higher contact area between the mesoporous oxide and the HTM. As a consequence, these combined effects result in a lower recombination resistance with a concomitant reduction in Voc. The notable reduction in the FF of the 40% single-step JV parameters supports this line of reasoning as well. However, all the single step solar cells present a similar Voc due to the difference in charge generation (reflected by the different Jsc), which compensate for the variations in their respective R_{rec}.
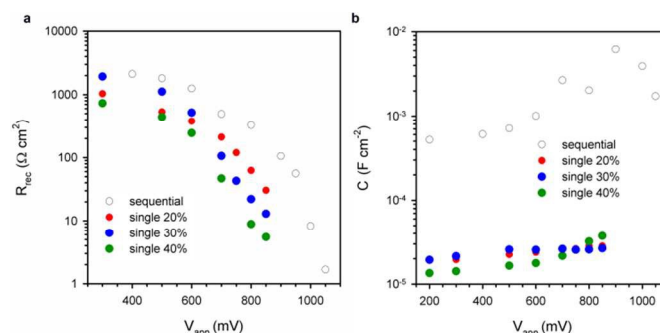
Figure 4 Parameters extracted from the IS fittings: **(a)** recombination resistance and **(b)** associated capacitance as function of forward bias

When observing the low frequency capacitances associated with the resistance (Figure 4b), a striking difference becomes apparent between the two different deposition processes. In the single step samples, the increase of the capacitance with the voltage is much lower, as similarly observed by Dualeh et al.[20] This observation is interpreted as a contribution of the compact TiO_2 capacitance in the low forward bias region, almost invariant with the potential, and at higher forward bias a charge accumulation in the mesoporous TiO_2 activated by the TiO_2/HTM contact (the values are in the expected order of magnitude for a capacitance related to charge accumulating within the mp-TiO_2). In contrast, the capacitance measured when utilizing the sequential deposition method is up to 100 times higher over the entire potential range, which indicates that different processes are involved when the perovskite over-layer is continuous. These high values of capacitance are still under debate, their origin being unclear. Nevertheless the recombination resistance associated with it seems to be the determining the JV curve. It is worthwhile to remark that the classical comparison of the recombination on the basis of the potential, (commonly performed in similar type of devices, such as DSC or OPV) cannot be applied here, since it requires an energetic reference against the DOS of the minority carrier transporting material. Therefore a proper model to further analyse the $CH_3NH_3PbI_3$ solar cell is still required.

Conclusions

To summarize we employed two different deposition techniques (sequential deposition and single step deposition with different precursor concentrations) to illustrate the effect of the perovskite over-layer on the solar device mechanisms. The sequential deposition method enables a better pore filling and the formation of a more conformal and structured capping layer on top of the perovskite compared to the single-step deposition technique. The contact areas between the HTM and perovskite and HTM and the TiO_2 are, thus, minimized and the shunting is reduced, reflected on the FF and Voc parameters. The improvement in Voc and FF observed for the sequential processing deposition technique is justified by a) a reduction of the recombination and b) an accumulation of charge within the perovskite absorber rather than in the mesoporous TiO_2.

Notes and references

[a] Energy Research Institute @NTU (ERI@N) Research Techno Plaza, 50 Nanyang Drive , 637553, Singapore E-mail: PBPablo@ntu.edu.sg

[b] School of Materials Science and Engineering Nanyang Technological University Nanyang Avenue , 639798 , Singapore.

[c] Laboratoire des sciences photomoléculaires, Ecole Polytechnique Fédérale de Lausanne, 1015 Lausanne, Switzerland.

[d] Laboratory for Photonics and Interfaces, Ecole Polytechnique Fédérale de Lausanne, 1015 Lausanne, Switzerland.

E-mail: thomas.moehl@epfl.ch; carole.graetzel@epfl.ch

[+] These authors contributed equally to this work.

1. H.-S. Kim, C.-R. Lee, J.-H. Im, K.-B. Lee, T. Moehl, A. Marchioro, S.-J. Moon, R. Humphry-Baker, J.-H. Yum, J. E. Moser, M. Graetzel and N.-G. Park, *Scientific Reports*, 2012, **2**.

2. M. Liu, M. B. Johnston and H. J. Snaith, *Nature*, 2013, **501**, 395-398.

3. J. Burschka, N. Pellet, S.-J. Moon, R. Humphry-Baker, P. Gao, M. K. Nazeeruddin and M. Grätzel, *Nature*, 2013, **499**, 316-319.

4. M. M. Lee, J. Teuscher, T. Miyasaka, T. N. Murakami and H. J. Snaith, *Science*, 2012, **338**, 643-647.

5. I. Chung, B. Lee, J. He, R. P. H. Chang and M. G. Kanatzidis, *Nature*, 2012, **485**, 486-489.

6. N. J. Jeon, J. H. Noh, Y. C. Kim, W. S. Yang, S. Ryu and S. I. Seok, *Nature Materials*, 2014, 1-7.

7. H. Zhou, Q. Chen, G. Li, S. Luo, T. b. Song, H. S. Duan, Z. Hong, J. You, Y. Liu and Y. Yang, *Science*, 2014, **345**, 542-546.

8. J.-H. Im, I.-H. Jang, N. Pellet, M. Grätzel and N.-G. Park, *Nat Nano*, 2014, **9**, 927-932.

9. NREL, Research Cell Efficiency Records, http://www.nrel.gov/ncpv/images/efficiency_chart.jpg.

10. G. Xing, N. Mathews, S. S. Lim, N. Yantara, X. Liu, D. Sabba, M. Grätzel, S. Mhaisalkar and T. C. Sum, *Nature materials*, 2014, **13**, 476-480.

11. T. Moehl, J. H. Im, Y. H. Lee, K. Domanski, F. Giordano, S. M. Zakeeruddin, M. I. Dar, L.-P. Heiniger, M. K. Nazeeruddin, N.-G. Park and M. Grätzel, *The Journal of Physical Chemistry Letters*, 2014, **5**, 3931-3936.

12. L. Gil-Escrig, G. Longo, A. Pertegas, C. Roldan-Carmona, A. Soriano, M. Sessolo and H. J. Bolink, *Chemical Communications*, 2015.

13. Z.-K. Tan, R. S. Moghaddam, M. L. Lai, P. Docampo, R. Higler, F. Deschler, M. Price, A. Sadhanala, L. M. Pazos, D. Credgington, F. Hanusch, T. Bein, H. J. Snaith and R. H. Friend, *Nat Nano*, 2014, **9**, 687-692.

14. O. Malinkiewicz, A. Yella, Y. H. Lee, G. M. Espallargas, M. Graetzel, M. K. Nazeeruddin and H. J. Bolink, *Nature Photonics*, 2013, **8**, 128-132.

15. H. Li, K. Fu, P. P. Boix, L. H. Wong, A. Hagfeldt, M. Grätzel, S. G. Mhaisalkar and A. C. Grimsdale, *ChemSusChem*, 2014, n/a-n/a

16. H. K. Mulmudi, N. Yantara, D. Sabba, M. Gratzel, S. G. Mhaisalkar, P. P. Boix and N. Mathews, *Chemical Communications*, 2013, **49**, 11089-11091.

17. J.-H. Im, H.-S. Kim and N.-G. Park, *Apl Materials*, 2014, **2**, 081510-081510.

18. M. H. Kumar, S. Dharani, W. L. Leong, P. P. Boix, R. R. Prabhakar, T. Baikie, C. Shi, H. Ding, R. Ramesh, M. Asta, M. Graetzel, S. G. Mhaisalkar and N. Mathews, *Advanced Materials*, 2014, **26**, 7122–7127.

19. T. Leijtens, S. D. Stranks, G. E. Eperon, R. Lindblad, E. M. J. Johansson, I. J. McPherson, H. Rensmo, J. M. Ball, M. M. Lee and H. J. Snaith, *ACS nano*, 2014.

20. A. Dualeh, T. Moehl, N. Tetreault, J. Teuscher, P. Gao, M. K. Nazeeruddin and M. Gratzel, *Acs Nano*, 2014, **8**, 362-373.

21. R. S. Sanchez, V. Gonzalez-Pedro, J.-W. Lee, N.-G. Park, Y. S. Kang, I. Mora-Sero and J. Bisquert, *The Journal of Physical Chemistry Letters*, 2014, **5**, 2357-2363.

22. V. Gonzalez-Pedro, E. J. Juarez-Perez, W.-S. Arsyad, E. M. Barea, F. Fabregat-Santiago, I. Mora-Sero and J. Bisquert, *Nano letters*, 2014, **14**, 888-893.

ChemComm Accepted Manuscript